RSC Advances

PAPER

View Article Online
View Journal | View Issue

Cite this: *RSC Adv.*, 2020, **10**, 8751

Naphthalimide based smart sensor for CN^-/Fe^{3+} and H_2S. Synthesis and application in RAW264.7 cells and zebrafish imaging†

Sanay Naha,[a] Shu-Pao Wu *[b] and Sivan Velmathi *[a]

Received 2nd October 2019
Accepted 20th February 2020

DOI: 10.1039/c9ra07998j

rsc.li/rsc-advances

Achieving selective detection of target analytes in aqueous media continues to be an arduous proposition. Herein, we report the conceptualization and synthesis of a novel tailor-fit molecular probe **R** based on 1,8-naphthalimide which acts as a trifunctional molecular sensor for CN^-, Fe^{3+} and H_2S. **R** shows colorimetric and fluorometric "on–off" relay recognition for CN^- (red colour and orange emission) and Fe^{3+} (no colour and no emission) in 5% H_2O + DMSO medium which is experimentally ascertained to be a tandem deprotonation–protonation process and is supported by ^{1}H-NMR titration. Among all RSS (Reactive Sulphur Species), **R** shows selectivity for H_2S through red colouration. Other coexistent anions, cations and RSS cause no discernible perturbation to the detection process. The detection of H_2S is attributed to a chemodosimetric reduction of the nitro to amino group as evidenced by a potentiometric titration assay. The experimental observations are well supported by DFT theoretical calculation. The K_a for CN^-/Fe^{3+} are 1.4×10^4 M^{-1}, 6.07×10^4 M^{-1} respectively and photochemical yield of **R** + CN^- is 0.86. Limit of detections for CN^-, Fe^{3+} and H_2S are 17.5 nM, 8.69 μM and 8.1 μM respectively. Receptor **R** is effective for real time applications, bio-compatible and has been successfully employed for confocal fluorescence imaging of RAW264.7 cell and zebrafish.

Introduction

There has been an unchecked increase in the release of toxic inorganic effluents from industrial sources into terrestrial water resources. This necessitates the development of techniques for the detection and quantification of inorganic pollutants. The adverse health consequences of ions such as cyanide, are well documented such as complications of vascular, visual, central nervous, cardiac, endocrine and metabolic systems.[1–8] Chemically, cyanide ion is a resilient nucleophile, sufficiently basic in nature, and can act as an ambidentate ligand and most importantly a pseudohalide. Cyanide is chosen as an exemplar since it finds widespread application in metallurgy, mining, electroplating and polymer synthesis.[9–11] According to the WHO guideline, the optimum tolerance limit of cyanide is 0.07 mg L^{-1} in drinking water and about 0.5–3.5 mg kg^{-1} of cyanide to an adult is lethal.[12]

Alongside cyanide, metals, specifically transition metals are copiously used for catalytic redox reactions in biological systems. Among transition metals, iron is the third most abundant metal ion present in humans and plays a pivotal role in oxygen transport, electron transport, balancing ionic pressure and is an integral part of the heme protein in our blood.[13,14] Like all inorganic ions, an untethered increase in iron concentration can prove harmful. Apart from ionic analytes, there are some neutral species available in waste which are equally dangerous to mankind. Of these, H_2S is predominant. Due to fungal activity and direct use, there has been a steady accumulation of H_2S in wastewater.[15–18] Therefore, methods for the quantitative and qualitative detection of cyanide, iron and H_2S assume ample significance.

Numerous well-established techniques are known for qualitative and quantitative estimation of analytes. These include atomic absorption spectroscopy (AAS),[19] inductively coupled plasma-mass spectroscopy (ICPMS),[20] inductively coupled plasma emission spectrometry (ICPES),[21] chromatography (HPLC and LC),[22] voltammetry[23] and so on. But these processes suffer from pitfalls such as frantic sample preparation procedures, requirement of sophisticated instrumentation, non-portability and high costs. Most of these processes are time-consuming. On the contrary, colorimetric and fluorescent sensors have marked advantages as they are easy to use, exhibit fast response times, involve simple synthetic procedures, are affordable, reusable, portable and most importantly involve real time bare-eye observation.

For detection, there are various strategies that have been adopted till date. These include single analyte and dual analyte

[a]*Organic and Polymer Synthesis Laboratory, Department of Chemistry, National Institute of Technology, Tiruchirappalli, India. E-mail: velmathis@nitt.edu*

[b]*Department of Applied Chemistry, National Chiao Tung University, Hsinchu, Taiwan. E-mail: spwu@mail.nctu.edu.tw*

† Electronic supplementary information (ESI) available. See DOI: 10.1039/c9ra07998j

detection. However, multifunctional receptors have not been equally explored. The development of multifunctional molecular sensors based on a single molecular structure has attracted a lot of attention in recent years.[24–31] In this regard, many reports are available which involve extensive investigations for the multifunctional sensor molecules towards cation–cation, or, anion–anion, or, anion–cation, or, cation–anion, or, ionic–neutral or neutral–ionic analytes combinations.[32] There are few reports available on Fe^{3+}–CN^- recognition.[33–38] However, triple analyte selective receptors are not common.[39]

Herein, we report a simple 1,8-naphthalimide based probe as tailor-fit triple action smart chemosensor **R** for the sequential detection of CN^- and Fe^{3+} *via* colorimetric and fluorometric 'on–off' method and H_2S through colorimetric method in semi-aqueous media over a wide pH range. DFT calculations supported the experimental findings and results are in correlation with experimental data. The receptor is capable of detecting analytes in biological systems. The results are documented in subsequent paragraphs.

Results and discussion

The receptor **R** was characterized using IR, ^1H & ^{13}C-NMR and HR-mass spectroscopic methods. The synthesized receptor **R** has an interesting molecular framework which consists of binary interacting sites. One is the amide moiety where a nucleophilic attack or deprotonation can take place, and another is the nitro functional group which is susceptible to reduction in the presence of reducing analytes (Scheme 1). Based on this assumption, the receptor was examined for triple action anion, cation and reactive species sensing in various solvents and investigated using UV-Visible, fluorescence, and ^1H-NMR spectroscopic techniques. Density Functional Theory (DFT) was employed for theoretical calculation to support the observed results. Prior to sensing studies, the dependence of receptor's efficiency in different solvents was determined. The receptor did not show appreciable effect in less-polar solvents like THF, toluene, MeOH, EtOH and DIOX. Rather, the receptor is quite efficacious in polar solvents like ACN, DMF and DMSO. Among polar solvents, the performance in DMSO is conducive for photo-physical studies (Fig. S5†).

Visual selectivity experiment

The receptor contains multiple heteroatoms which can provide satisfactory binding sites for metal ions and on this note the receptor was exempted for naked eye cation recognition. But, there was no specificity and selectivity for a particular cation, as none of the metal ions show any significant interference neither by colorimetric nor by emissive approaches. Subsequently, the receptor is applied for anion selectivity and to do so, 2 equivalents of all anions such as CN^-, F^-, Cl^-, Br^-, I^-, AcO^-, HSO_4^-, $H_2PO_4^-$, NO_3^-, OH^-, ClO_4^-, H_2S, N_3^- and PF_6^- were added to 3 mL (15 μM) of **R** solution in DMSO. Among the library of anions, only CN^- selectively shows an intense and drastic color change from no colour to an intense red and an orange fluorescence 'turn-on'. Alongside CN^-, H_2S also shows rapid and intense colour change to red colour but without any 'turn-on' emission. Other anions like I^- AcO^-, HSO_4^-, $H_2PO_4^-$, NO_3^-, SCN^-, N_3^- and ClO_4^- show a bright golden-yellow emission but no change in colour (Fig. S6†). After determining the effect of water on CN^- detection *via* emissive mode (Fig. S7 and S8†), a sensing medium of 5% aqueous DMSO is used, where only CN^- selectively and specifically shows an intense red colouration and orange emission 'turn-on' (Fig. 1). The change in color and 'turn-on' of fluorescence can be attributed to deprotonation of the acidic hydrazide [–NH].

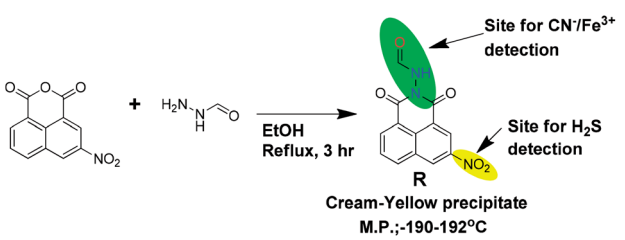

Scheme 1 Synthetic route and probable detection cites of R.

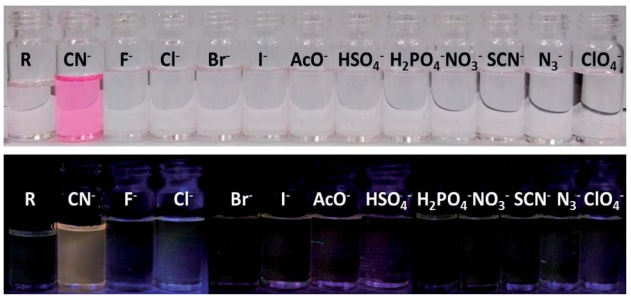

Fig. 1 Bared eye colour change and turn-on emission under UV-light for cyanide in 5% aqueous-DMSO solvent.

Electronic and emission response

The spectroscopic responses were recorded for anion sensing studies which depicted the selectivity for cyanide among competitive anions. The electronic spectra of receptor in 5% aqueous solution shows two absorption peaks at around 280 nm due to σ–σ* transition and 332 nm due to π–π* transition and almost all the anions in the chosen ensemble yield the same trends in their corresponding electronic spectra. In the case of cyanide, the peak position of σ–σ* transition does not change but the intensity reduces abruptly followed by the disappearance of the 332 nm peak. Along with that, the appearance of a peak around 530 nm is attributed to n–π* transition of the de-protonated receptor and the drastic change in colour is justified (Fig. 2a). On deprotonation, the formed negative charge leads to the red shift in λ_{max}, and this shift in λ_{max} is conspicuously correlated with the molecular orbitals and the energy of transition from HOMO to LUMO. On the other hand, the emission spectrum is self-explanatory for cyanide selectivity which proceeds *via* 'turn-on' emission. On excitation at 530 nm, an emission is observed at λ_{em} 563 nm,

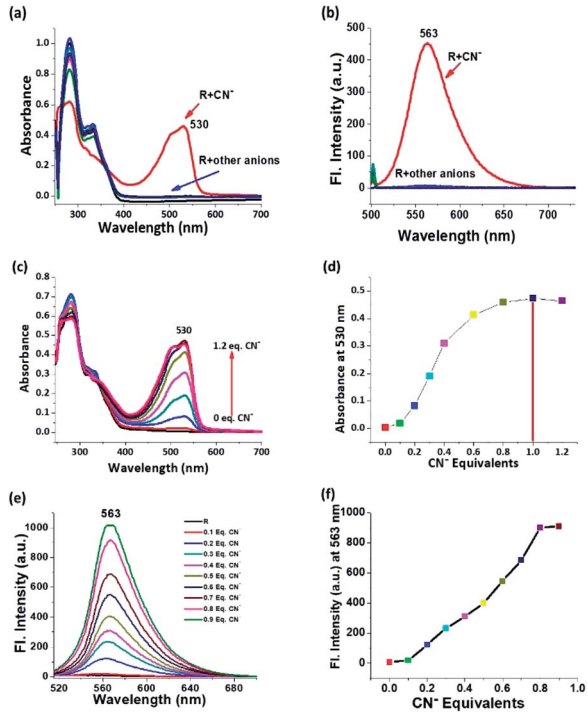

Fig. 2 (a) Electronic and (b) emission spectral response of receptor **R** with all anions in 5% aqueous medium; (c) incremental titration of receptor **R** by cyanide by electronic technique; (d) plot of cyanide concentration *vs.* absorbance at 530 nm for each addition; (e) incremental titration of receptor **R** by cyanide by emission spectroscopy and (f) plot of cyanide concentration *vs.* emission intensity at 563 nm for each addition.

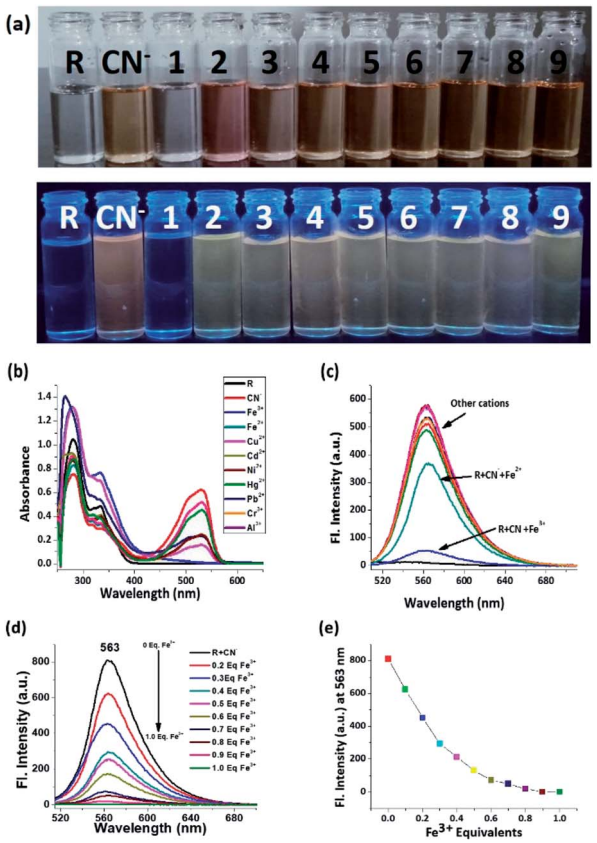

Fig. 3 (a) Naked eye image and image under UV-light of Fe^{3+} selectivity by **R** + CN^- *via* both decolouration and quenching of emission where 1 = Fe^{3+}, 2 = Fe^{2+}, 3 = Cu^{2+}, 4 = Cd^{2+}, 5 = Ni^{2+}, 6 = Hg^{2+}, 7 = Pb^{2+}, 8 = Cr^{3+} and 9 = Al^{3+}. (b) Electronic and (c) emission response of **R** + CN^- with all cations; (d) incremental titration of **R** + CN^- by Fe^{3+} by emission spectroscopy and (e) plot of Fe^{3+} concentration *vs.* emission intensity at 563 nm for each addition.

which is the region for orange emission (Fig. 2b). Titrimetric analysis of the receptor *via* both UV-Vis and fluorescence methods shows a saturation limit of receptor with one equivalent of cyanide, and on further addition, no appreciable change is observed (Fig. 2c–f). The receptor is selective and specific for CN^- even in the presence of other competing analytes (Fig. S9†).

Relay recognition experiment

As the receptor shows optimum specificity for cyanide, the **R**–CN^- ensemble was employed for the sequential recognition of cationic analytes and the cyanide treated receptor is capable of recognizing Fe^{3+} *via* both decolorization and rapid 'turn-off' emission which is evident from the colour change from intense red to colourless and the quenching of orange emission under UV-light (Fig. 3a). Other metal ions did not show any comparative interference in this context. From the electronic spectrum it can be inferred that the absorption peak at around 332 nm reappears and the peak at 530 nm disappears upon introduction of Fe^{3+} (Fig. 3b). Similarly, in the emission spectrum, the intensity of **R** + CN^- is decreased by 12 fold after Fe^{3+} addition (Fig. 3c). In the titration between **R** + CN^- *vs.* Fe^{3+}, the decrease of emission intensity follows a specific pattern and at 1 equivalent of Fe^{3+} concentration, emission gets quenched completely. On further addition, no discernible change is observed (Fig. 3d and e).

Naked eye H_2S selectivity

Since the receptor is tailor-made for H_2S sensing due to the presence of a nitro group, the receptor is examined for interference from other reactive sulphur species (RSS). And as expected, the receptor precisely and selectively shows an intense colorimetric response only for H_2S (Fig. 4a). The electronic spectra illustrate the specificity of the probe towards H_2S. The appearance of a new peak at 560 nm is attributed to the formation of an amine chromophore (Fig. 4b). Both cyanide and H_2S show an intense red colouration, but the absorption peak position for H_2S is red shifted by almost 30 nm when compared to CN^- (Fig. 4c). Incremental titration of receptor **R** by H_2S shows a saturation limit of 1 equivalent. It can therefore be said that the chemodosimetric reduction of the nitro group follows a 1 : 1 stoichiometric ratio (Fig. 4d).

pH effect

The effect of pH on the sensitivity and efficacy of a receptor is an important factor that needs to be consider while developing

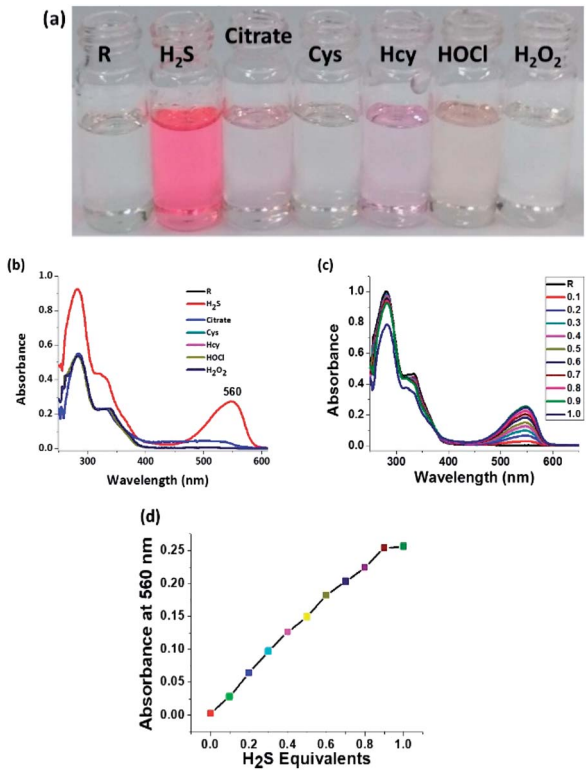

Fig. 4 (a) Naked eye image of H_2S selectivity among all RSS and ROS by R *via* colorimetric output, (b) electronic response of receptor R with all RSS and ROS, (c) incremental titration of receptor R by H_2S by electronic technique and (d) plot of H_2S concentration *vs.* absorbance at 560 nm for each addition.

a molecular probe. The bio-applicability of a receptor invariably depends on pH. So, to examine pH effect, 3 mL of 15 μM solution of **R** in various pH values were prepared using HEPES buffer and the emission of each pH solution was recorded before and after addition of CN^-. The receptor **R** showed an intense orange emission in the pH range from 7 to 11, which can be attributed to the stability of the deprotonated **R** in that pH range. Since the reason behind emission is the deprotonation, basic medium certainly supports deprotonation of acidic/replaceable protons. The receptor **R** is therefore efficient within a range of pH 7 to 11 and can be used for fluorescence cell imaging of CN^- (Fig. 5).

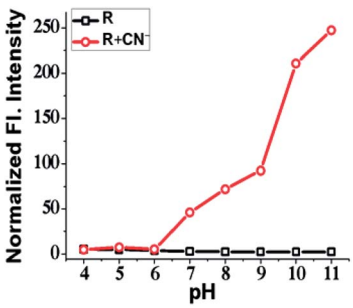

Fig. 5 Plot of emission intensity between only receptor R and R + CN^- in different pH at 563 nm.

Quantitative calculation

The authenticity of a developed analytical method is always evaluated on the basis of suitability and sustainability of its intended purpose, recovery, standardization requirements, sensitivity and specificity, ease of analysis, skill subset required, time and cost. Limit of detection is an important performance characteristic of any analytical method. These parameters stand to describe the smallest concentration of an analyte that can be reliably measured by an analytical method. Job's plot for CN^- and Fe^{3+} showed a 1 : 1 stoichiometry for the sensing process (Fig. S10†). However, since H_2S detection involves a chemodosimetric reduction process, a Job's plot construction is not applicable since no stable binding is taking place. The calculated association constants (K_a) for sequential recognition of CN^-/Fe^{3+} are 1.4×10^4 M^{-1} and 6.07×10^4 M^{-1} respectively. Limit of detection (LOD) for CN^-, Fe^{3+} and H_2S are found to be 17.5 nM, 8.69 μM and 8.1 μM respectively (Fig. S11, S12 and S13) (Table S1†). The standard iodometric method for standardization of H_2S dissolved in water has been opted for reference and according to the iodometric method, the concentration of H_2S used for quantification is found to be 10 μM which is well correlated to known limits. Hence, this method can be considered as an efficient approach for H_2S detection. The quantum yield of CN^-/Fe^{3+} recognition process has been calculated with respect to rhodamine B. The quantum yields (ϕ) for **R**, **R** + CN^- and **R** + CN^- + Fe^{3+} are 0.01, 0.86 and 0.01 respectively (Table S2†).

Lifetime experiment

According to the emission spectra, the emission maxima of **R** + CN^- is at 563 nm and to perform luminescence lifetime decay experiment a 550 nano-LED source was used. The average decay time of the excited state of only **R** was found to be 0.2 ns. After the addition of 10 μM of CN^- ions to **R**, the average luminescence lifetime of **R** + CN^- increased to 0.3 ns. When this was followed by the addition of 10 μM Fe^{3+} to the resultant **R** + CN^- solution, the average lifetime again decreased and revert back to 0.2 ns. The lifetime decay curve of only **R**, **R** + CN^- and **R** + CN^- + Fe^{3+} were fitted to a triple-exponential decay curve using theoretical calculations. The 0.1 ns resultant increment of the average lifetime before and after addition of cyanide implies

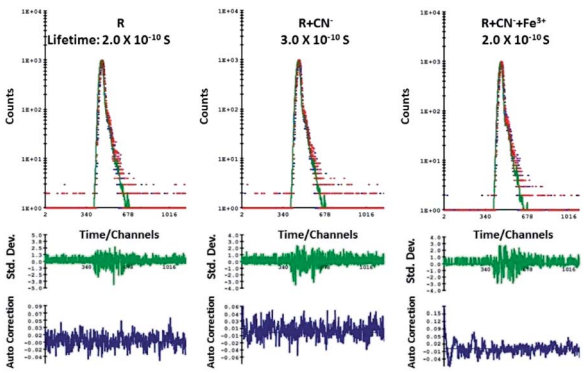

Fig. 6 Lifetime experiment of only R, R + CN^- and R + CN^- + Fe^{3+}.

that the excited state of '**R** + CN^-' is comparatively stable in comparison to the excited state of free receptor **R**. As a result, there is a delay of 0.1 ns in the decay rate, when cyanide ion deprotonates the receptor; hence it is proved that there is a scope for the enhancement of fluorescence in the case of **R**–CN^- interaction. Whereas, the resultant decrement of average lifetime after addition of Fe^{3+} to the deprotonated **R** is 0.1 ns, which implies that the increase in decay rate and hence quenching of emission is favorable (Fig. 6).

Theoretical studies

Theoretical calculations were performed for only **R**, deprotonated **R** and reduced **R** to support the deprotonation process taking place upon introduction of cyanide and the reduction of nitro group to amine group by H_2S. The structural optimization and quantum mechanical calculations were performed using Gaussian 09 software. The Gauss View 5 GUI was used for visualization of results. Geometry optimizations for ground state of only **R** and reduced **R** were conducted using DFT/B3LYP/6-31g basis set and excited state of deprotonated **R** was conducted using TD-DFT/B3LYP/6-31g basis set alongside solvent effect of DMSO respectively. Highest occupied molecular orbital (HOMO) and lowest unoccupied molecular orbital (LUMO) for the respective form of **R** were generated from their optimized structures (Fig. 7a and b). The calculated energy gap between HOMO and LUMO of only **R** is 3.08 eV which after deprotonation of amide –NH by cyanide ions decreases to 2.1 eV (excited state of deprotonated **R**). Similarly, the energy gap between HOMO and LUMO of only **R** and reduced **R** also decreases to 2.15 eV from 3.08 eV. The calculated energy for only **R**, deprotonated **R** and reduced **R** corresponds to wavelengths of 402 nm, 589 nm and 576 nm respectively and well coincided with the experimental values.

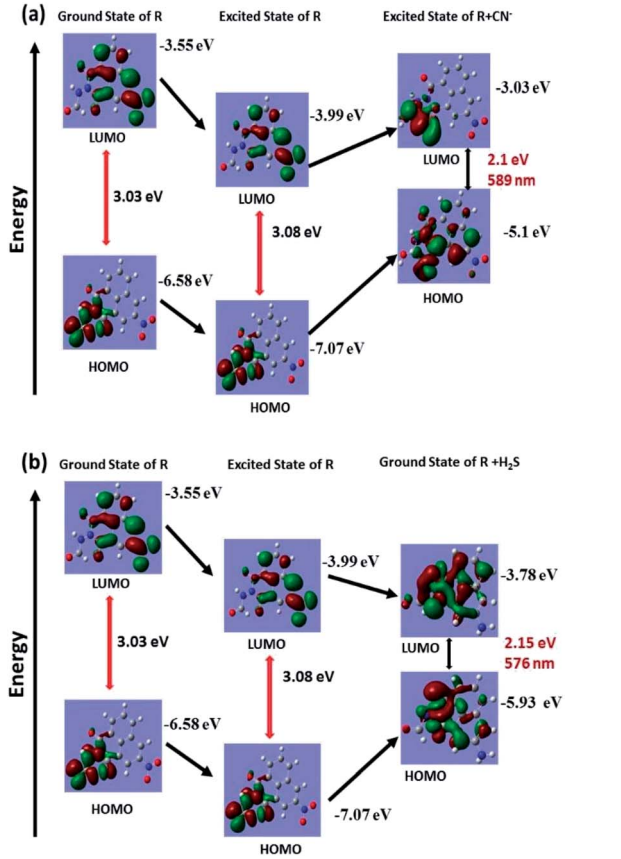

Fig. 7 Theoretical calculation for ground state and excited state energy of (a) receptor R and R + CN^- for cyanide recognition and (b) receptor R and R + H_2S for H_2S recognition.

^{1}H-NMR titration

The successive detection of cyanide and Fe^{3+} by **R** was supported by ^{1}H NMR titration. A solution of **R** (0.01 M in DMSO-d_6), TBACN (0.01 M in DMSO-d_6) and $FeCl_3$ (0.01 M in DMSO-d_6) were used for the ^{1}H NMR titrations (Fig. 8). In the NMR spectrum, the peak at 11 ppm corresponds to the only acidic [–N–H] proton present in the receptor and on addition of 1 equivalent cyanide ion to **R**, the peak at 11 ppm disappears. Furthermore, the peak position of aldehyde proton is shifted downfield due to the localization of the electronic field. On addition of CN^-, the obvious dense electron density around the napthalimide moiety has no discernible impact on its proton signals in the ^{1}H NMR spectra. Due to the lack of extended conjugation, the accrued negative charge on N-atom in the molecular framework got static dissipation. As a result, the molecule does feel the electron density over a specific position which results in an internal charge transfer (ICT) process. It follows, upon addition of Fe^{3+} to the resultant mixture, regeneration of [–NH] appears at around 10.9 ppm which confirms the binding of cyanide with Fe^{3+}.

Potentiometric titration

The reductive chemodosimetric approach adopted by the receptor for H_2S sensing is supported by potentiometric titration and recorded using a cyclic voltammeter. In aqueous solutions, H_2S exists either as HS^- or even as S^{2-} which impart significant reducing character and current flow. In a typical experiment, Pt electrodes were used as both working and counter electrodes and Ag/AgCl electrode was used as a reference electrode. The three electrodes were dipped in a 10 μM 20 mL aqueous solution, the oxidation–reduction potential of the resultant cell assembly was measured. Only H_2S solution shows a reduction potential of −0.5 V with a current of

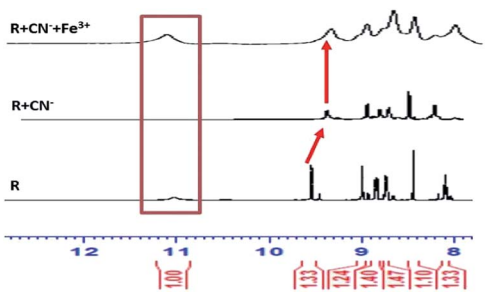

Fig. 8 ^{1}H-NMR titration of receptor **R** with CN^-/Fe^{3+} analyte pair for relay recognition mechanism.

−0.00135 mA. On sequential addition of 1.1 equivalent receptor **R** to the H_2S solution, the concentration of reduced sulphur decreases as evidenced by the decrease in current from −0.00135 mA to −0.0006 mA and the receptor **R** gets saturated at one equivalent of H_2S (Fig. 9a). The reduction peak for H_2S becomes sharper towards the end of the addition and ultimately linearity is observed (Fig. 9b). Hence, the reduction of the nitro group in receptor by H_2S is evident.

Sensing mechanism

From UV, PL spectroscopy, ^{1}H-NMR titration, potentiometric titration and theoretical calculations, it is ascertained that deprotonation of [–NH] proton by cyanide ions is the driving force for the sensing action of the receptor. From the sequential titration plot, it is confirmed that the saturation limit of the **R** is 1 equivalent of cyanide. The molecular framework of the receptor facilitates an ESIPT mechanism between the adjacent carbonyl oxygen and the [–NH] group on excitation rendering the receptor non-emissive. Upon deprotonation, there is a formation of a negatively charged species in which a delocalization of negative charge through resonance is curtailed. Therefore, the only tool available for charge dissipation is amide–imine tautomerism which results in the attenuation of ESIPT and switches on the ICT mechanism. The result is the appearance of an intense orange emission at 563 nm. The introduction of Fe^{3+} to the emissive system results in the protonation of the receptor, thereby effectively inhibiting ICT due to the absence of free cyanide in the solution (Fig. 10). The sensing of H_2S in purely chemodosimetric and does not affect ESIPT. The only discernible change was the reduction of the nitro group on the receptor. As a result, there is only a color change from colorless to red but no emission.

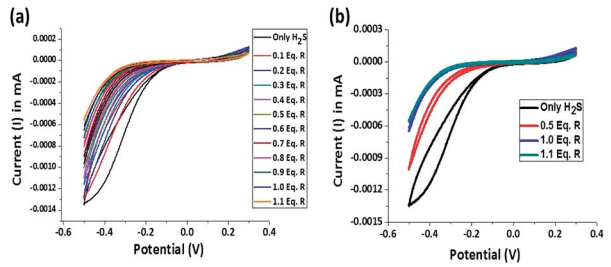

Fig. 9 (a) Potentiometric titration of receptor **R** and H_2S and (b) a correlative plot of potential for only H_2S, after 0.5 equivalent of **R**, after 1.0 equivalent of **R** and after 1.1 equivalent of **R**.

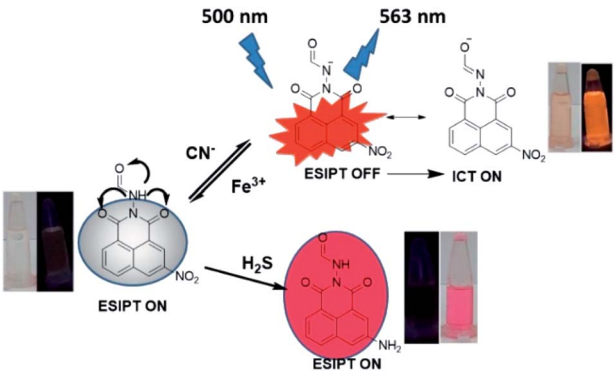

Fig. 10 The probable sensing mechanism for relay recognition of CN^-/Fe^{3+} and chemodosimetric sensing of H_2S.

Application

To ascertain the employability of the receptor **R** for real-world applications, three different tests were considered. The pH effect studies showed that the receptor is effective within the biological pH range. Subsequently, a strip-test was performed to assess the relay recognition of CN^-/Fe^{3+}. H_2S etching was used for real-sample analysis. A cytotoxicity (MTT) assay of **R** was also performed to test the viability of the molecule for biological applications. And finally, the receptor was used for confocal fluorescence imaging of RAW264.7 cells and zebrafish for relay recognition of CN^-/Fe^{3+}.

Real sample

Since the receptor **R** showed selectivity and specificity for CN^-/Fe^{3+} ions and H_2S in semi-aqueous media without any interference, **R** was applied for colorimetric and fluorometric naked eye observable strip-test analysis. A 15 μM solution was prepared in 9 : 1 acetone–DMSO solvent. The filter papers were coated with the receptor solution and dried in a hot-air oven at 70 °C for about 2 hours. On the dry paper strips, cyanide was added and immediately an intense red colour was observed (Fig. 11a) along with an orange emission which was instantly quenched by Fe^{3+}. The addition of Fe^{3+} produced a feeble yellowish colour on the paper strips. This was attributed to the presence of $FeCl_3$ (Fig. 11b). For the H_2S strip test, a solution of H_2S is used as ink and then the letters 'NCTU' were inscribed on the dried strip using a paintbrush (Fig. 11c and d). The strip test for CN^-/H_2S was validated using various concentration of CN^-/H_2S ranging from (0.1–10) μM (Fig. S14†).

Cell imaging

The cell line RAW264.7 were cultured on 18 mm glass-cover slips in Dulbecco's modified Eagle's medium (DMEM) supplemented with fetal bovine serum (10% FBS) at 37 °C under 5% CO_2 atmosphere and allowed to adhere for 24 h. After washing with PBS, the

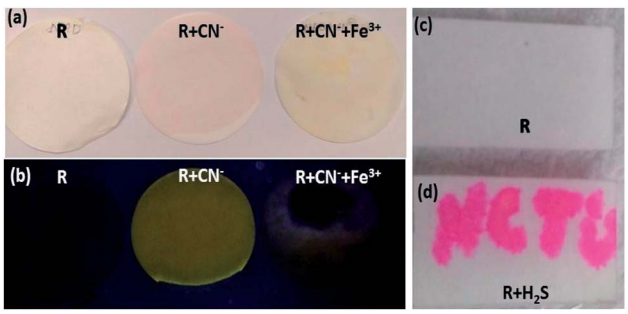

Fig. 11 (a) Naked eye colour change of the receptor coated strips for CN^-/Fe^{3+} sequential selectivity, (b) the 'off–on–off' emission response for CN^-/Fe^{3+} sequential selectivity on strips and (c) TLC plate anchored with receptor **R** and (d) H_2S is used as ink.

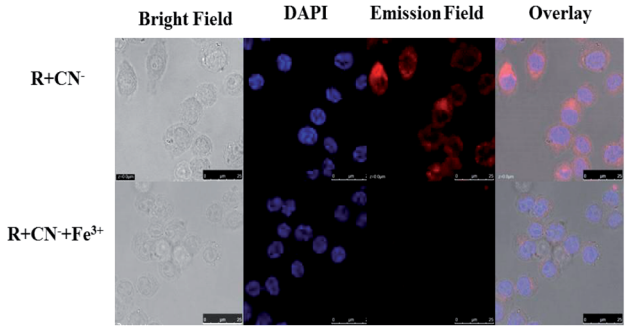

Fig. 12 The confocal fluorescence RAW264.7 cell imaging for sequential recognition of CN^- and Fe^{3+} *via* 'on–off' emission response.

setup was incubated for another 30 min with **R** (20 μM) in DMEM. After washing the excess **R** using PBS, **R** + RAW264.7 cells were incubated with CN^- (10 μM) for 30 min. To assess CN^- ion uptake, the cells were treated with CN^- (10 μM in 2 mL) dissolved in sterilized PBS at pH 7.4 and incubated for 30 min at 37 °C and 5% CO_2 atmosphere. The treated cells were washed using PBS (2–3 mL) to remove remaining CN^- ions. 2 mL of culture media was added to the cell culture, which was treated with a 10 mM solution of **R** (10 mM, 2 mL) dissolved in DMSO. The samples were incubated at 37 °C for 30 min. After removing the culture media and followed by washing with PBS, confocal images were recorded. From the images, it could be inferred that **R** has very good permeability through the RAW264.7 cell membrane and the receptor does not possess any emission. Whereas **R** sensed CN^- selectively with 'turn-on' orange fluorescence which again gets quenched on introduction of Fe^{3+} (Fig. 12).

Zebrafish imaging

The eggs of zebrafish were subjected to a 3 day maturation period and subsequently used for confocal fluorescence imaging experiment. Firstly, the zebrafish were placed in 2 mL of 15 μM solution of receptor to allow for a smooth intake and then rested for 30 min at room temperature. After the standby period, the fishes were washed 2–5 times with deionized water and fluorescence images were recorded. It is obvious that the receptor is not inherently emissive in the fish. The cleaned fishes were treated with 2 mL of 15 μM solution of cyanide and allowed for another 30 min. Then again after cleaning the fishes, the fluorescence images were recorded. The fish show red emission and the intensity of the emission is maximum in the stomach region. After this, the fish were again treated with 2 mL of 15 μM Fe^{3+} ($FeCl_3$ solution) and fluorescence images were recorded. The intense red emission is quenched completely upon the introduction of Fe^{3+}. These tests show that the receptor can be used as a cyanide marker for *in vivo* applications and can precisely indicate the presence of Fe^{3+} ions (Fig. 13).

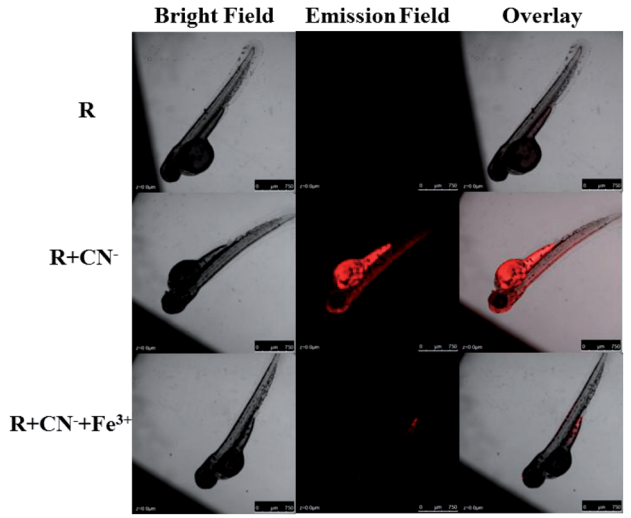

Fig. 13 The confocal fluorescence zebrafish imaging for sequential recognition of CN^- and Fe^{3+} *via* 'off–on–off' emission response.

Experimental

Materials and instrumentations

3-nitro-1,8-napthalimide and formic hydrazide were purchased from Sigma-Aldrich and used as received. The solvents used for synthesis and photophysical studies were of spectroscopic grade. For photophysical studies double-distilled water was used and pH of water was 6.7 and conductivity was 30 dS m^{-1}. For stock solution of all anions tetrabutylammonium salts were purchased and for all cations, chloride salts were used. Bruker DRX-300, Agilent Unity INOVA-500 and Bruker Ascend 500 NMR spectrometer were used for NMR spectral characterization. UV-Vis spectra were obtained using Agilent 8453 UV-Vis spectrometer and Shimadzu UV-2600 spectrophotometer. Fluorescence spectra measurements were obtained from Hitachi F-7000 fluorescence spectrophotometer and Shimadzu RF5301pc spectrofluorophotometer. The potentiometric titration was measured using Bio-logic SP-150 cyclic-voltammeter (CV). Lifetime measurement studies were done at Horiba Delta time instrument coupled with TCSPC. Fluorescent images were taken on a Leica TCS SP5 X AOBS and Leica TCS SP5 II Confocal fluorescence microscope. The cells RAW264.7 were provided by the Food Industry Research and Development Institute (Taiwan). The cell imaging and zebrafish imaging experiments were conducted in strict accordance with the guidelines provided by Govt. of Taiwan and was approved by Institutional committee (NCTU, Taiwan).

Spectroscopic procedures

The stock solution of receptor **R** (1.0×10^{-3} M in DMSO) was prepared and kept at room temperature. Then the stock solution was diluted with 5% (H_2O + DMSO) to a final concentration of 2.5×10^{-5} M for spectral analysis. All anion, cations and RSS stock solutions were prepared in the concentration of 5×10^{-3} M in water. ROS and RSS were prepared freshly and used.

Synthesis of R

In a hot-dry 100 mL round bottom flask, 15 mL ethanol solution of 3-nitro-1,8-napthalimide (486 mg, 2 mM) was prepared and stirred vigorously at 78 °C for 15 min. To the resultant clear

solution, 10 mL ethanolic solution of formic hydrazide (130 mg, 2.1 mM) was added dropwise over a time period of 10 min. The resultant mixture was set for reflux for 3 h. The reaction mixture was allowed to cool to room temperature followed by 20 mL of diethylether was added and kept in room temperature for 12 h. A cream-yellow precipitate was obtained which was separated through filtration and washed with hot water, hot ethanol, then product was dried in vacuum oven. The compound was further purified using ethyl acetate wash followed by re-crystallization in methanol–acetonitrile (9 : 1) medium (Scheme 1). Yield of the reaction is 530 mg (92%).

Melting point: (190–192) °C.

FT-IR (cm^{-1}): 3421 (absorbed water, KBr), 3198 (Ar–C–H), 3076 and 2922 (═NH), 1735 (C═O, amide), 1700 and 1664 (C–N, amide) (Fig. S1†).

^1H δ (500 MHz; DMSO-d_6; TMS): 11.025 (s, 1H), 9.578 (s, 1H), 9.015 (s, 1H), 8.879–8.863 (d, 1H, $J = 8$), 8.759–8.746 (d, 1H, $J = 7$), 8.436 (s, 1H) and 8.13–8.099 (t, 1H, $J = 8$).

^{13}C ppm (125 MHz; DMSO-d_6; TMS): 161.16, 160.79, 160.28, 146.38, 137.70, 135.23, 131.62, 131.06, 129.90, 129.82, 124.30, 123.91 and 122.53 (Fig. S3a and b†).

135-DEPT ppm (125 MHz; DMSO-d_6; TMS): 137.69, 135.22, 131.04, 129.89 and 124.29 (Fig. S3c†).

LCMS (HR-MS) m/z: calcd for $C_{13}H_7N_3O_5$, 285.0386, found: 284.0313 [M − H] (Fig. S4†).

Conclusions

In summary, we have successfully developed a triple action smart receptor which can detect quantitatively and qualitatively CN^- and Fe^{3+} *via* a relay recognition pathway and H_2S through a reductive chemodosimetric mechanism without any interference from other analytes in 5% H_2O–DMSO media. The receptor senses the analytes effectively and efficiently within permissible limits. The CN^-/Fe^{3+} and H_2S sensing mechanisms are supported by ^1H-NMR and cyclic voltammetric titrations. Quantum mechanical calculations using DFT support the experimental findings. The receptor is employed in strip-tests for the detection of CN^-/Fe^{3+} *via* both naked eye colorimetric and fluorometric response along with writing ink for H_2S. Since the receptor is bio-compatible and non-toxic, it is capable in detecting CN^-/Fe^{3+} in RAW264.7 cells and zebrafish *via* confocal fluorescence imaging.

Conflicts of interest

Authors have no conflict of interest.

Acknowledgements

Author Sanay Naha is highly thankful to Department of Science and Technology, India (DST-India) for providing financial support through INSPIRE Fellowship (IF150881), TEEP internship program and NCTU, Taiwan for research infrastructure.

References

1 V. Kumar, H. Rana and M. P. Kaushik, *Analyst*, 2011, **136**, 1873.
2 X. Wu, B. Xu, H. Tong and L. Wang, *Macromolecules*, 2011, **44**, 4241.
3 C. O. Ng, S. W. Lai, H. Feng, S. M. Yiu and C. C. Ko, *Dalton Trans.*, 2011, **40**, 10020.
4 M. D. Holaday, G. Tarafdar, B. Adinarayana, M. L. P. Reddy and A. Srinivasan, *Chem. Commun.*, 2014, **50**, 10834.
5 S. Wang, H. Xu, Q. Yang, Y. Song and Y. Li, *RSC Adv.*, 2015, **5**, 47990.
6 C. Aebersold, B. Amstutz, A. E. Steuer, T. Kraemer and F. Zelder, *Anal. Methods*, 2015, **7**, 9707.
7 G. Balamurugan and S. Velmathi, *Anal. Methods*, 2016, **8**, 1705.
8 S. Suganya, J. S. Park and S. Velmathi, *J. Fluoresc.*, 2016, **26**, 207.
9 V. Bhalla, H. Singh and M. Kumar, *Dalton Trans.*, 2012, **41**, 11413.
10 C. Männel-Croisé and F. Zelder, *Anal. Methods*, 2012, **4**, 2632.
11 J. Isaad, F. Malek and A. El Achari, *RSC Adv.*, 2013, **3**, 22168.
12 Y. Singh and T. Ghosh, *Talanta*, 2016, **148**, 257.
13 W. H. Organization, *Guidelines for drinking-water quality*, 3rd edn, 2004, vol. 1, p. 339.
14 Y. Yue, F. Huo, C. Yin, J. Chao and Y. Zhang, *Sens. Actuators, B*, 2015, **212**, 451.
15 S. Mardanya, S. Karmakar, D. Mondal and S. Baitalik, *Dalton Trans.*, 2015, **44**, 15994.
16 N. Thirumalaivasan, P. Venkatesan and S. P. Wu, *New J. Chem.*, 2017, **41**, 13510.
17 B. Zhao, Y. Yang, Y. Wu, B. Yang, J. Chai, X. Hu and B. Liu, *Sens. Actuators, B*, 2018, **256**, 79.
18 C. B. da Silva, E. S. Gil, F. d. S. Santos, A. M. Moras, L. Steffens, P. F. B. Goncalves, D. J. Moura, D. S. Ludtke and F. S. Rodembusch, *J. Org. Chem.*, 2018, **83**, 15210.
19 S. Mardanya, S. Karmakar, M. Bar and S. Baitalik, *Dalton Trans.*, 2015, **44**, 21053.
20 Z. Q. Hu, X. M. Wang, Y. C. Feng, L. Ding, M. Li and C. S. Lin, *Chem. Commun.*, 2011, **47**, 1622.
21 A. Balamurugan and H. Lee, *Macromolecules*, 2015, **48**, 3934.
22 J. B. Chae, H. J. Jang and C. Kim, *Photochem. Photobiol. Sci.*, 2017, **16**, 1812.
23 H. J. Jang, H. M. Ahn, M. S. Kim and C. Kim, *Tetrahedron*, 2017, **73**, 6624.
24 B. Zhao, T. Liu, Y. Fang, L. Wang, W. Kan, Q. Deng and B. Song, *Sens. Actuators, B*, 2017, **246**, 370.
25 Q. Lin, F. Zheng, T. T. Lu, J. Liu, H. Li, T. B. Wei, H. Yao and Y. M. Zhang, *Sens. Actuators, B*, 2017, **251**, 250.
26 P. S. Nayab and M. Shkir, *Sens. Actuators, B*, 2017, **245**, 395.
27 T. Zhou, X. Chen, Q. Hua, W. Lei, Q. Hao, B. Zhou, C. Su and X. Bao, *Sens. Actuators, B*, 2017, **253**, 292.
28 N. Narayanaswamy and T. Govindaraju, *Sens. Actuators, B*, 2012, **161**, 304.
29 Q. Fu, G. Chen, Y. Liu, Z. Cao, X. Zhao, G. Li, F. Yu, L. Chen, H. Wang and J. You, *Analyst*, 2017, **142**, 1619.

30 P. Zhang, X. Nie, M. Gao, F. Zeng, A. Qin, S. Wu and B. Z. Tang, *Mater. Chem. Front.*, 2017, **1**, 838.
31 Y. Singh and T. Ghosh, *Talanta*, 2016, **148**, 257–263.
32 S. Suganya, S. Naha and S. Velmathi, *ChemistrySelect*, 2018, **3**, 7231.
33 D. Yun, J. M. Jung and C. Kim, *Inorg. Chim. Acta*, 2018, **479**, 154.
34 W. Wang, J. Wu, Q. Liu, Y. Gao and B. Zhao, *Tetrahedron Lett.*, 2018, **59**, 1860.
35 A. Mohammadi and S. Yaghoubi, *Sens. Actuators, B*, 2017, **241**, 1069.
36 R. Kumar, V. Bhalla and M. Kumar, *Dalton Trans.*, 2013, **42**, 8808.
37 L. Wang, W. T. Li, W. J. Qu, J. X. Su, Q. Lin and M. Zhang, *Supramol. Chem.*, 2017, **7**, 489.
38 G. Punithakumari and S. Velmathi, *J. Photochem. Photobiol., A*, 2019, **373**, 94.
39 N. Vijay, G. Balamurugan, P. Venkatesan, S. P. Wu and S. Velmathi, *Photochem. Photobiol. Sci.*, 2017, **16**, 1441.